J. Fluid Mech. (1991), *vol.* 222, *pp.* 329–350
Printed in Great Britain

Experiments on transition to turbulence in oscillatory pipe flow

By DAVID M. ECKMANN AND JAMES B. GROTBERG

Biomedical Engineering Department, The Technological Institute, Northwestern University, Evanston, IL 60208, USA *and* Department of Anesthesia, Northwestern University Medical School, Chicago, IL 60611, USA

(Received 5 May 1989 and in revised form 21 May 1990)

A laser-Doppler velocimeter is used to analyse volume-cycled oscillatory flow of a Newtonian viscous fluid in a straight circular tube. The axial velocity is measured at radial positions across the diameter of the tube for a wide range of amplitude A = stroke distance/tube radius ($2.4 \leqslant A \leqslant 21.6$) and Womersley parameter ($9 < \alpha < 33$). Transition to turbulence is detected during the decelerating phase of fluid motion for $500 < R_\delta < 854$, where $R_\delta = \alpha A \sqrt{2}$ is the Reynolds number based on Stokes-layer thickness. The turbulence is confined to an annular region which is a few times the Stokes-layer thickness near the wall. Hot-film anemometer measurements indicate the core flow remains stable when the boundary layer becomes turbulent for R_δ up to 1310.

1. Introduction

Understanding the processes of heat and mass transport in oscillatory flow is a topic of interest for many applications ranging from tidal estuaries (Smith 1982) and novel heat exchangers (Kurzweg 1985) to the field of pulmonary physiology. For example, high-frequency ventilation apparently involves a different mechanism of gas transport in the conducting pulmonary airways than that associated with conventional ventilation. High-frequency ventilators deliver tidal volumes an order of magnitude smaller at frequencies one or two orders of magnitude higher than those delivered by conventional ventilators, and they maintain adequate respiratory gas exchange (Slutsky *et al.* 1980). In order to model gas exchange, respiratory physiologists have drawn on results of theoretical transport studies by Watson (1983) for straight tubes, Eckmann & Grotberg (1988) for curved tubes and Godleski & Grotberg (1988) for tapered tubes, as well as the experimental work of Joshi *et al.* (1983) for oscillatory flow in straight circular tubes. These investigations consider only laminar convection–diffusion processes. In addition to the laminar mixing phenomena, it has been hypothesized that transport of gases through the airways could be substantially augmented by the chaotic velocity fluctuations associated with the generation of turbulence during high-frequency ventilation (Fredberg 1980).

In the volume-cycled oscillatory flows common to respiratory situations, the straight-tube system is governed by two dimensionless parameters: the Womersley parameter, $\alpha = a(\omega/\nu)^{\frac{1}{2}}$, a ratio of vorticity diffusion time to period of oscillation; and the amplitude, $A = V_T/(\pi a^3)$. Here, a is the tube radius, ω is the angular frequency, ν is the kinematic viscosity and V_T is the tidal volume. Previous investigators, including Hino, Sawamoto & Takasu (1976) and Ohmi *et al.* (1982) have characterized

the resulting flow using the parameter α and either the Reynolds number $R = Ua/\nu$ or $R_\delta = U\delta/\nu$, where U is the cross-section mean of the peak velocity amplitude, and $\delta = (2\nu/\omega)^{\frac{1}{2}}$ is the Stokes-layer thickness. If $U = \omega d$ (d is the stroke distance $V_T/\pi a^2$) is chosen as the velocity scale for volume-cycling of the flow, then, in terms of the parameters we have defined above, $R_\delta = \sqrt{2}\alpha A$ and $R = 2\alpha^2 A$.

For $\alpha \gg 1$ a Stokes layer develops in the tube and several studies of its stability have been made. Collins' (1963) linear-theory analysis of the stability of a Stokes layer predicts a critical Reynolds number $R_\delta = 21.4$, assuming a quasi-static flow with a steady basic state. This value of R_δ was determined to be incorrect, however, by von Kerczek & Davis (1972) who numerically integrate the Orr–Sommerfeld equation and determine that the critical Reynolds number for transition, based on a quasistatic profile, is $R_\delta = 56.3 \pm 3$. Von Kerczek & Davis (1972), using energy theory, find that the flow of a Stokes layer in a semi-infinite medium must be absolutely stable against two-dimensional disturbances for $R_\delta < 38.9$. Additionally, for general three-dimensional disturbances, they find that absolute stability is assured for $R_\delta < 19.0$. The full time-dependent linear stability theory of von Kerczek & Davis (1974) predicts stability to infinitesimal disturbances in the range $0 \leqslant R_\delta \leqslant 800$, $\alpha = 5.66$ for a flow confined between two infinite parallel plates, one of which is oscillating tangentially. Although no calculations are done for $R_\delta > 800$, the authors suggest that the Stokes layer may be stable for all R_δ within the realm of linear theory. They note that finite-amplitude subcritical instabilities are possible. Yang & Yih (1977) consider theoretically the stability of a pressure-cycled oscillatory pipe flow subjected to small amplitude, axially symmetric perturbations. Results of Floquet theory and numerical analysis show that the flows are stable for all modes and wavenumbers considered up to Reynolds numbers of 2000 where the lengthscale is the radius a and the velocity scale is $(|\partial p/\partial x| a/\rho)^{\frac{1}{2}}$.

Li (1954) examined experimentally the viscous boundary layer of a deep fluid layer above an oscillating plate and determined that the critical boundary layer for transition to turbulence is $R_\delta = 566$. Transition was identified by visual observation of dye marker dispersion near the solid boundary. Rapid longitudinal scattering of the marker fluid indicated that the boundary layer had become turbulent. Sargeev (1966) investigated a bellows-generated oscillatory flow in a circular tube for $4 \leqslant \alpha \leqslant 40$. He observed transition to turbulence in the boundary layer occurring at $R_\delta = 500$ for flow conditions having a developed Stokes layer ($\alpha > 5$). Measurements on the power input to the bellows and observation of aluminium powder within the fluid were used to assess transition. Merkli & Thomann (1975) made hot-wire velocimeter measurements of transition to turbulence in a piston driven oscillating flow in an air-filled resonance tube closed at one end over a range of combinations of amplitude ($0.6 \leqslant A \leqslant 2.9$) and Womersley parameter ($40 \leqslant \alpha \leqslant 70$). Turbulent bursts occurred during the decelerating phase of fluid motion, and these were always followed by relaminarization of the flow. In no case was turbulence observed during an entire cycle. Onset of turbulence as recorded by the hot-wire probe, which was fixed near the wall, was not uniquely described by $R_\delta =$ constant, as expected, but, as shown by flow visualization, it appeared to be hastened by the presence of the hot-wire element for increased frequency of oscillation. From the results of these flow-visualization experiments they concluded that the occurrence of turbulence is characterized by R_δ, since different experimental parameter settings yielded the same critical value of $R_\delta = 283$ when no hot-wire probe resided in the flow.

Hino *et al.* (1976) made hot-wire measurements at various radial positions in a volume-cycled oscillatory flow in a straight circular tube. The experimental

parameter ranges investigated were restricted to large A ($3.4 \leqslant A \leqslant 400$) and smaller α ($1.91 \leqslant \alpha \leqslant 8.75$). The flow was characterized into three regimes: (*a*) a laminar regime with no observed instability; (*b*) a weakly turbulent regime in which small-amplitude disturbances were observed in the hot-wire output throughout the cross-section; and (*c*) a conditionally turbulent regime in which large-scale velocity fluctuations occurring during the deceleration phase of fluid motion were recorded at all radial positions. From this study it appears that, during transition, the instability arises only during the decelerating phase, while in the accelerating phase the flow recovers to laminar flow, confirming the similar finding of Merkli & Thomann (1975). Hino *et al.* (1976) detect high-frequency velocity disturbances during deceleration at all radial locations investigated from the midline to the wall for $R_\delta = 550$, $\alpha \leqslant 5.5$.

In subsequent experiments utilizing hot-wire techniques in oscillating pipe flow, Ohmi *et al.* (1982) find both acceleration phase and deceleration phase turbulence throughout the cross-section for $7.4 < \alpha < 41$ and $R_\delta > 1000$. The region of parameter space describing transition to turbulence is not mapped out for large α, though, since this study considers only $R_\delta < 439$ and $R_\delta > 604$ for $\alpha > 8.8$. Moreover, the detail of the local measured velocity as a function of time is not presented for these values of α which are larger than those investigated by Hino *et al.* (1976).

Hino *et al.* (1983) used hot-wire and laser-Doppler velocimeter techniques to examine the generation of turbulence in a reciprocating rectangular wind-tunnel flow with $\alpha = 18.1$, $R_\delta = 876$, which is well beyond the critical value for transition. They concluded that turbulence is generated near the wall during the decelerative phase of fluid motion and that the turbulent eddies generated are convected toward the channel midline. These findings are consistent with the results of studies of oscillatory U-tube channel flows conducted by Hayashi & Ohashi (1982) using flow visualization and hot-wire anemometry in the parameter range $57 < \alpha < 68$ and $878 \leqslant R_\delta \leqslant 996$ and by Sumer, Jensen & Fredsoe (1987) using laser-Doppler anemometry at $\alpha = 132$, $R_\delta > 3000$.

Left unanswered by these experimental studies is whether or not there exists a flow regime at large α and near transition in which the boundary layer is unstable while the inviscid core region remains turbulence free. At first glance, one would not expect the appearance of turbulence in the core plug flow environment at or near transition. Three experiments are discussed in this paper which address aspects of this issue. The first experiment, presented in §3, is designed to identify the parameter range over which transition to turbulence occurs and to demonstrate whether or not, on transition to turbulence, the core region in a volume-cycled oscillatory pipe flow retains its structure as an inviscid plug showing no instability. Velocities are measured by laser-Doppler velocimetry (LDV). A second experiment, described in §4, using LDV was conducted to ascertain whether transition to turbulence occurs at lower values of R_δ when a dummy hot-wire probe resides in the flow field. The results of this experiment are compared to the results of the first experiment to identify the effect of the hot-wire probe on the flow field, with particular attention given to the central region of the tube. As detailed in §5, a third experiment was conducted utilizing a hot-film anemometer to measure the flow near the wall and in the central region of the tube. These measurements are made for purposes of comparison to LDV results made with and without the dummy probe resident in the flow.

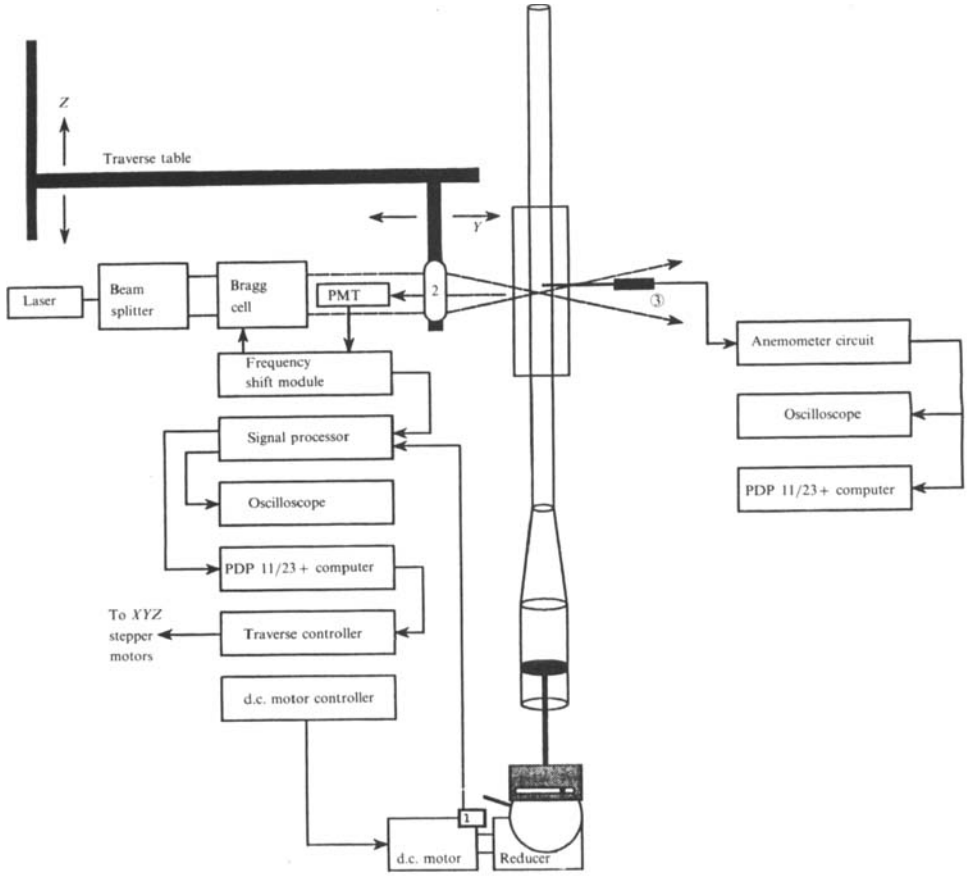

FIGURE 1. The experimental apparatus and data acquisition system. 1. Optical encoder; 2. Objective lens; 3. Hot-film probe.

2. Experimental methods

The experimental test section consists of two Plexiglas plates bolted together. At the centre of the rectangular cross-section and down the 10 in.-long axis a circular cylinder of diameter $D = 1.25$ in. has been bored. At each end of this cylinder there is a counter-bore cut to accommodate the connecting tubes. The two Plexiglas connecting tubes have an inner diameter of 1.25 in. to match the circular cylinder bored through the test section. Experiments of Gerrard & Hughes (1971) show that laminar flow in front of an oscillating piston is fully developed at a distance $L = 0.03\ DR_\delta$ away from the piston. Based on this criterion and on preliminary measurements, the connecting tubes used are of sufficient length for the flow to be fully developed when it enters the test section for $R_\delta < 900$. We found, however, as discussed in §5, that in our apparatus the flow in the test section was free of entrance vorticity effects to much larger values of R_δ.

One end of each tube inserts tightly into the counter-bores located at the ends of the test section. The top tube is open to the atmosphere while the bottom tube is inserted into a Plexiglas cylinder out of which a conical section has been cut. At one end of the conical section the diameter matches the inner diameter of the connecting tube. Here a counter-bore has been cut for insertion of the connecting tube. The conical section has a taper angle of 3.86° increasing to a diameter of 2.165 in. The

taper angle is slender to prevent separation of the flow in thc conical section. This tapered section gives a 3:1 reduction in cross-sectional area allowing shorter piston displacements. The large-diameter end of the conical section connects to an aluminium cylinder of matching inner diameter. The piston rides in this cylinder.

The piston drive rod and two additional guide rods pass through ball bushings and terminate in the scotch yoke assembly to be described. The guide rods and ball bushings, not drawn in figure 1, serve to reduce the rocking tendency of the piston as it is driven back and forth in the cylinder. The entire apparatus is securely mounted vertically on a sturdy table and tethered to a unistrut frame which is bolted to the tabletop.

A sinusoidal drive mechanism was constructed to allow piston motion with nine discrete amplitudes (eccentric tapped holes are located every 0.250 ± 0.001 in. from 0.250 in. to 2.250 in. on the drive wheel) over a range of angular frequencies. The mechanism consists of a variable-speed electric motor paired with a speed reduction gear, a motor speed controller, and a scotch yoke to translate the rotational motor motion into the linear vertical displacement of the piston assembly. The motor and reduction gear combinations used were a $\frac{1}{3}$-horsepower Indiana General 1725 r.p.m. variable-speed motor with a 50:1 Boston Gear model U118-50 speed reducer and a $\frac{1}{2}$-horsepower Indiana General 1750 r.p.m. variable-speed motor with a 20:1 Boston Gear model 718-20-J speed reducer. In both cases the motor speed was regulated by a Fincor model 2351 adjustable speed d.c. motor control. The two independent parameters in the experiments, A and α, are selected by the settings of the drive mechanism. The amplitude A is determined by the eccentric position of the cam drive while α is determined by the drive wheel period of oscillation, which is resolved to ± 5 ms with the triggering device described below. The other quantities in each of these parameters are held fixed in the experiments.

An aqueous solution of potassium thiocyanate (KSCN) was chosen as the working fluid for the LDV studies, since the salt concentration could be easily adjusted to allow index of refraction matching between the Plexiglas and the fluid to within 0.05%, thus effectively eliminating the curved optical interface between the media. The fluid was found to be Newtonian with an average viscosity $\mu = 3.27$ cP when subjected to a range of shear rates using a Wells–Brookfield micro viscometer model LVT-C/P. The density of the fluid was measured to be $\rho = 1.426$ g/cm^3, giving a kinematic viscosity of $\nu = 0.0229$ cm^2/s. This is in good agreement with the value $\nu = 0.0225$ cm^2/s which was measured with a bulb viscometer.

We used a TSI model 9100-7 laser-Doppler velocimeter with a fibre optic link. General features of the system used in these experiments are: (i) Coherent INNOVA 70 4 watt argon ion laser operating at 514.5 nm; (ii) TSI model 9180A frequency shift module consisting of model 9182 Bragg cell and model 9186A power supply; (iii) model 9400 XYZ traverse mechanism; (iv) model 9160 photomultiplier system; (v) system 1980B counter type signal processor including model 1984B input conditioner and model 1985B period timer. The objective lens in these experiments is mounted on a three-axis traverse table with mirror mounts. The position of the traverse table is directed by a model 9430 position controller and is accurate to within 0.05 mm. Careful aligning techniques are used so that the traverse axes coincide with the axes of the test section. Reflected light from KSCN precipitate seed particles present in the flow is focused onto the photodetector assembly in backscatter mode. Signals from the photomultiplier tube are processed by the signal counter.

A TRW OPB847 slotted optical switch mounted on the motor assembly plates, shown in figure 1, is used to generate an external synchronization pulse desired in the

experimental set-up. Mounted on the drive wheel of the motor assembly is a switching pin which passes through the switch slot once per revolution. The pulse generated by the switch is recorded by the signal counter and is also used to determine the piston assembly period of oscillation. A Cambridge Digital PDP 11/23+ computer running the TSI-DRP3 software package is used to position the traverse table and to acquire data from the signal processor, which sends digital information through an interface cable to a direct memory access board in the computer. A general view of the data acquisition system is also presented in figure 1.

As a precaution to allow proper warm-up of the motor assembly and laser, the motor was allowed to run for a minimum of 15 min before any data collection was initiated. Data samples were acquired at 1 mm radial increments from the tube centre to approximately 3 mm from the wall and then in 0.5 mm increments to the edge of the boundary layer. The traverse direction was along the Y-axis, from tube centre toward the front face of the test section, keeping X and Z constant. Data were recorded at each radial position for a minimum of 10 oscillations, and in most cases from 10 to 12 oscillations with approximately 100 data points per cycle were captured in the data set. In some cases when the boundary layer was very thin ($\delta < 1$ mm) it was possible for the measuring volume to occupy a large portion of the region. Large velocity gradients existed across the probe volume in such a case and no reliable record of the velocity could be made. Owing to the dimensions of the measuring volume axes (0.28 mm along Y, 0.08 mm along both X and Z), when trying to measure very close to the wall the results were double-checked by traversing the measuring volume to the same radial position near the sidewall (moving in the Y-direction to the tube centre and then moving along the X-axis, holding Y and Z constant). The measuring volume having its minor axis oriented normal to the tube wall occupies less of the boundary layer than the measuring volume having its major axis normal to the tube wall.

Data files containing velocity information were plotted graphically on the computer screen as velocity versus time. This inspection of the experimental results was performed to check for sinusoidality and to examine the data for signs of the onset of turbulence. Data files were transferred to the Cyber 845 computer where they were regressed using the IMSL nonlinear regression subroutine RNLIN-/DRNLIN. This subroutine calculates the least-squares fit of two column data to a nonlinear regression model of the form:

$$y_i = f(x_i; \phi) + \epsilon_i \quad (i = 1, 2, \ldots, n), \tag{2.1}$$

where the observed values of the y_i constitute the values of the dependent variable, the known x_i are the values of the independent variables, ϕ is the vector of p regression parameters, and the ϵ_i are independently distributed normal errors with mean zero and variance σ^2.

Predictions from the laminar theory of oscillatory flow in a straight tube show that at any dimensionless radial location $r = r^*/a$, the axial velocity is given as:

$$w(r, \omega t) = \frac{J_0(i^{\frac{3}{2}}\alpha)}{4J_2(i^{\frac{3}{2}}\alpha)}\left[\frac{J_0(i^{\frac{3}{2}}\alpha r)}{J_0(i^{\frac{3}{2}}\alpha)} - 1\right] e^{i\omega t} + \text{c.c.}, \tag{2.2}$$

where J_n is the nth-order Bessel function of the first kind and c.c. denotes the complex conjugate. Equation (2.2) can be written in the form:

$$w(r, \omega t) = \phi_1(r) \cos[\omega t - \phi_2(r)], \tag{2.3}$$

where $\phi_1(r)$ is the amplitude, $\phi_2(r)$ is the phase angle and ω is the angular frequency. The data files were regressed to this nonlinear form where w and t are the two-column data in the experimental data file and the ϕ are the amplitude and phase angle predicted by the laminar theory. Output from this subroutine gives best-fit values of the vector ϕ and the sum of the squares of errors. The output values of ϕ are compared to the input values to determined if there is a large discrepancy.

We define $w'(r, \omega(t+kT))$ as the difference of the measured instantaneous velocity from the expected value $w(r, \omega t)$ given by (2.3), so it represents the velocity fluctuations around a zero mean. T is the period of oscillation and $k = 0, 1, 2, \ldots$. Since the data are not sampled at regular time intervals by the LDV, the values of $\omega(t+kT)$ are windowed to encompass every 3° of cam rotation. The values of w' were found not to vary if this was done for every 2° or 1° of rotation but this choice saves computation time. The standard deviation, σ, of the experimental data over the oscillatory cycle is given by:

$$\sigma(r, \omega t) = (\overline{w'^2})^{\frac{1}{2}} = \left[\frac{1}{M}\sum_{k=0}^{M-1} w'^2(r, \omega(t+kT))\right]^{\frac{1}{2}}, \tag{2.4}$$

where M is the number of consecutively sampled piston oscillations.

3. Results

3.1. *Preliminary studies*

We considered that the fluid may not remain well mixed in the vertical column and that solutal density gradients may cause convective flows to occur. After the fluid has been at rest overnight, measurements of index of refraction do not show a distinguishable difference between fluid extracted from the top of the tube and fluid drained from the bottom of the tube. The same is true when samples are taken after the motor drive has been running for two hours. Thus, it is reasonable to assume that any density gradients are small and that convective flows attributable to them are insignificant.

Thermal effects from local heating of the stagnant fluid were also investigated. Cooper *et al.* (1985) demonstrated that LDV heating of a recirculating liquid flow could have a significant influence. In their experiments, the onset of instability in an unsteady circular Couette flow was dependent on localized laser-induced thermal effects. As an experiment preliminary to our oscillatory flow measurements, the laser beams were focused in the fluid for an hour without the motor drive running. The measured velocity signals appeared as noise and had a time averaged mean of less than 0.5 mm/s with a smaller standard deviation. This velocity is much smaller than the comparatively large-amplitude imposed fluid motion. Therefore it is likely that any thermally-induced flows caused by local laser heating of the fluid or natural convection induced by temperature gradients in the laboratory frame are of little consequence in our experiments. Further, the heat imparted to the fluid will probably dissipate radially into the surrounded fluid and the residence time for liquid heating will diminish during the oscillatory cycling. We conclude from these checks that the velocity measurements made are undisturbed by local heating and fluid density stratification driving convective flows.

Measurements were made at fixed radial distance from the tube centre to check for axisymmetry of the flow at $\alpha = 17.9$, $A = 9.6$, $R_\delta = 243$. There was no appreciable difference in the velocity for fixed Z and r at angular locations spaced every 30°

		$\phi_1(r)$ cm/s		$\phi_2(r)$ radians	
	r^*/a	Theory	Expt	Theory	Expt
A	0	1.96	1.92	1.408	1.410
	0.48	2.03	2.05	1.430	1.433
	0.68	2.14	2.10	1.325	1.318
	0.88	1.54	1.60	0.958	0.962
	0.94	0.94	0.97	0.788	0.786
B	0	41.49	42.02	1.479	1.479
	0.76	44.14	44.63	1.462	1.462
	0.82	44.64	45.09	1.378	1.377
	0.92	34.62	34.95	1.075	1.075
	0.94	29.09	29.44	0.988	0.986
C	0	125.72	127.41	1.518	1.517
	0.29	125.72	127.05	1.518	1.517
	0.48	125.73	127.36	1.518	1.517
	0.68	125.45	126.92	1.518	1.516
	0.76	125.68	124.88	1.528	1.516

A $R_\delta = 34.3$, $\alpha = 10.1$, $A = 2.4$, $\delta/a = 0.140$, $\omega = 0.911$
B $R_\delta = 456$, $\alpha = 16.8$, $A = 19.2$, $\delta/a = 0.084$, $\omega = 2.513$
C $R_\delta = 854$, $\alpha = 28.0$, $A = 21.6$, $\delta/a = 0.051$, $\omega = 6.981$

TABLE 1. Theoretical data and regressed experimental data

around the tube axis. These measurements were made at radial positions in the inviscid core flow and in the boundary layer close to the wall to enable us to discern any asymmetry in the flow. It was also important to verify that there were no edge effects caused by mismatching of the inner diameter of the connecting tubes with the test section in the region of insertion. This was checked by moving the measuring probe vertically to a position 2 mm away from each of the test-section-measuring tube interfaces and collecting the same type of axisymmetry data as before. The measured flows compared well to the theoretically predicted velocities for laminar flow, so the edge effects are considered negligible.

3.2. *Oscillatory flow measurements*

Shown in table 1 is a sample of the theoretical and regressed experimental values of ϕ_1 and ϕ_2. The values of the dimensionless Stokes-layer thickness, scaled on the tube radius, and the piston assembly angular frequency, ω, are given. These values are tabulated at all r for each (α, A)-data measurement point used in the experiments.

Our results show that the measured amplitudes of the motion are generally 1–2% higher than the theoretical predictions. Discrepancies between the predicted values and the velocity measurements are most probably due to small machining errors leading to an increase in the actual volume displaced by the piston assembly from the anticipated volume displacement for a given rotary cam position. The phase information, however, is very nearly exact. The measured angular alignment is well within 1° of rotation, and small differences from the predicted phase are probably due to our inability to achieve greater resolution in aligning the peak piston position with triggering of the optical encoder device.

Figure 2(*a–d*) illustrates our ability to recover the basic state laminar velocity profiles. Velocity profiles are given for four combinations of α and A. The data points shown are derived by calculating the regressed velocities from (2.3) at the three instants in time, $\omega t = 0, \frac{1}{4}\pi$ and $\frac{1}{2}\pi$. Also drawn in this figure are the equation (2.2)

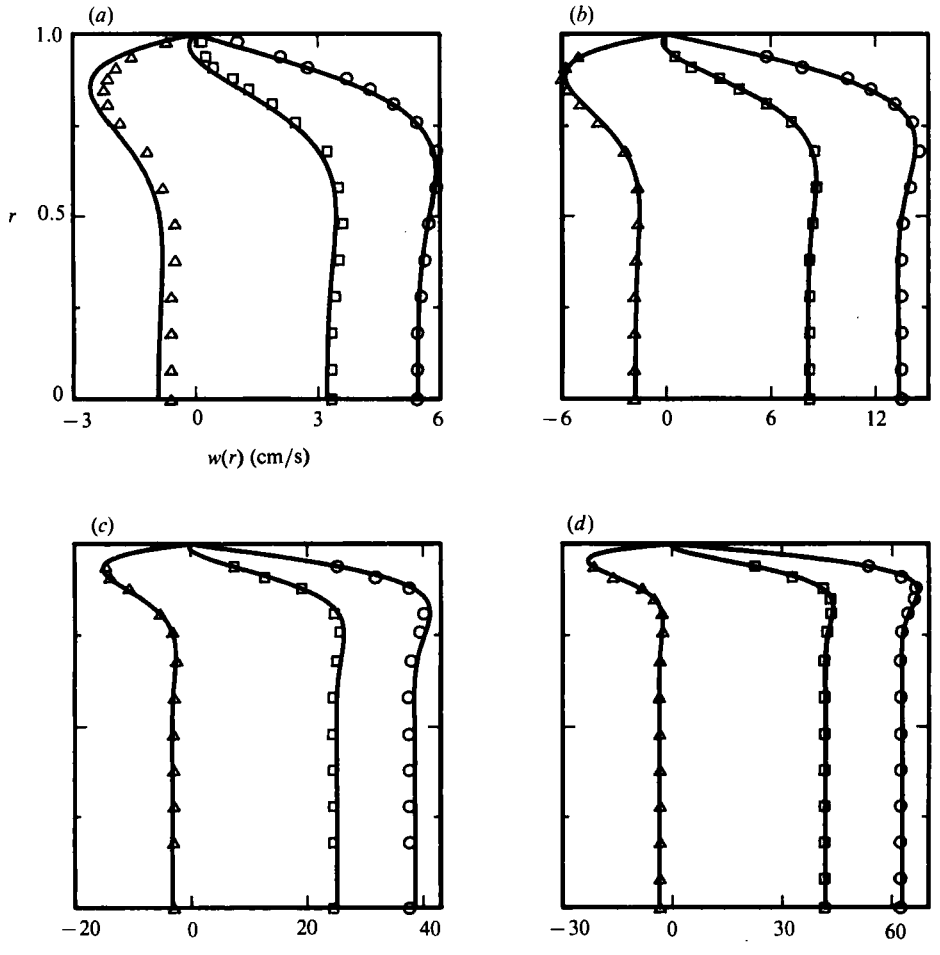

FIGURE 2. Basic state laminar velocity profiles measured by LDV. Phases shown are: ○, $\omega t = 0$; □, $\omega t = \frac{1}{4}\pi$; △, $\omega t = \frac{1}{2}\pi$. (*a*) $\alpha = 9.8$, $A = 7.2$, $R_\delta = 100$; (*b*) $\alpha = 11.9$, $A = 12.0$, $R_\delta = 202$; (*c*) $\alpha = 18.8$, $A = 14.4$, $R_\delta = 382$; (*d*) $\alpha = 26.5$, $A = 12.0$, $R_\delta = 450$. Solid lines are theoretical predictions.

theoretically predicted velocity profiles, shown as solid lines. That we can measure very near the wall and elucidate the features of the thin boundary layer for large α is evident in figure 2(*d*).

An example of the time history of the velocity at a fixed radial location is given in figure 3. Here a sample of the raw data from single-burst experimental measurements made at $r = 0$ for $\alpha = 16.8$, $A = 19.2$ and $R_\delta = 456$ are displayed. The data points appear tightly clustered in the shape of a sine wave, and the corresponding computed $\sigma(0, \omega t)$, plotted in figure 4(*a*), is shown to be 1.26 cm/s and relatively independent of the phase. This is 4.2% of U_{rms}, the root mean square velocity, and represents noise in the signal most probably due to mechanical vibrations, rather than turbulence, since the vorticity in the pipe flow is phase dependent. Figures 4(*b–e*) demonstrate that $\sigma(r, \omega t)$ remains constant at approximately this value and phase independent throughout the oscillatory cycle at all radial positions investigated.

At larger R_δ we also observe the core flow data to be sinusoidal with little scatter. Figure 5 shows the raw LDV data as a function of time at the dimensionless radial

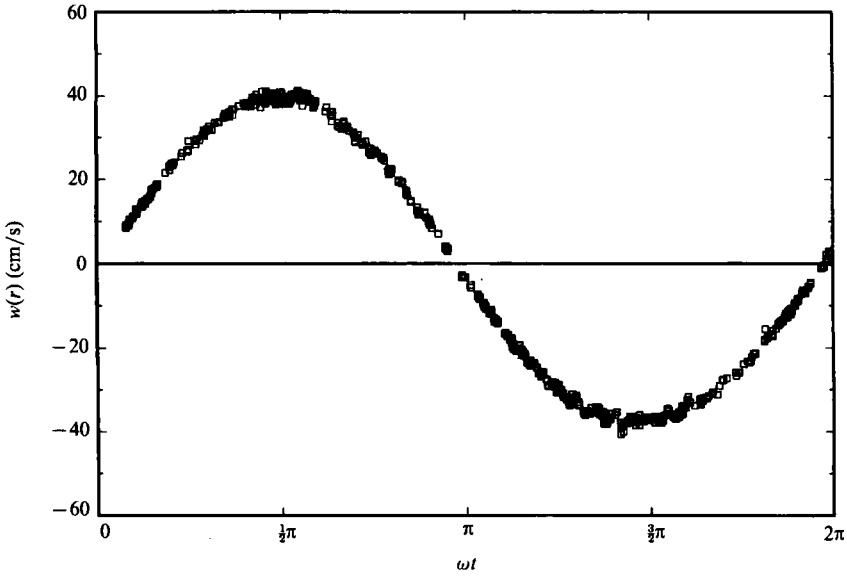

FIGURE 3. Laminar LDV velocity measurement made at dimensionless radial position $r = 0$ for $\alpha = 16.8$, $A = 19.2$, $R_\delta = 456$.

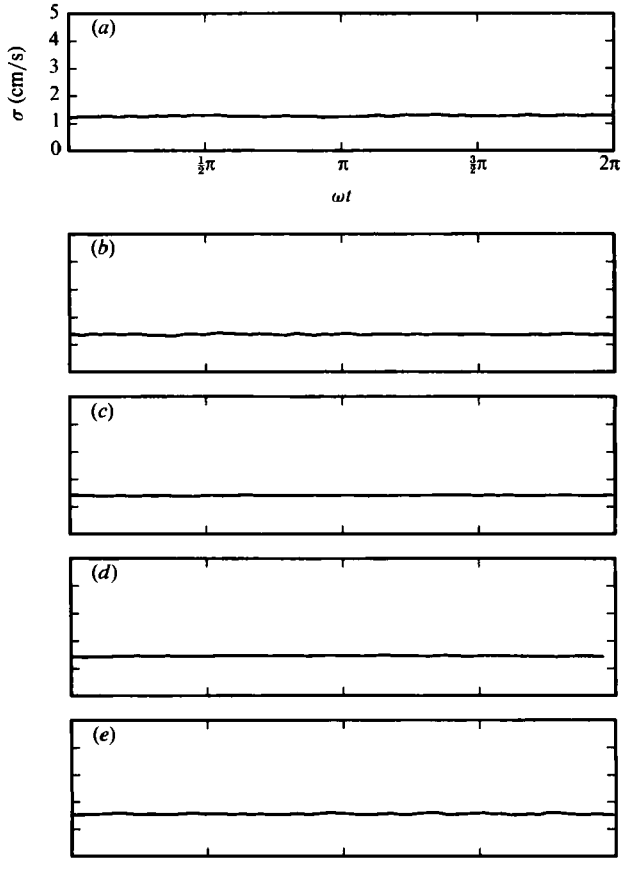

FIGURE 4. $\sigma(r, \omega t)$ for $\alpha = 16.8$, $A = 19.2$, $R_\delta = 456$, $\delta/a = 0.084$. (*a*) $r = 0$. (*b*) $r = 0.76$. (*c*) $r = 0.85$. (*d*) $r = 0.88$. (*e*) $r = 0.94$.

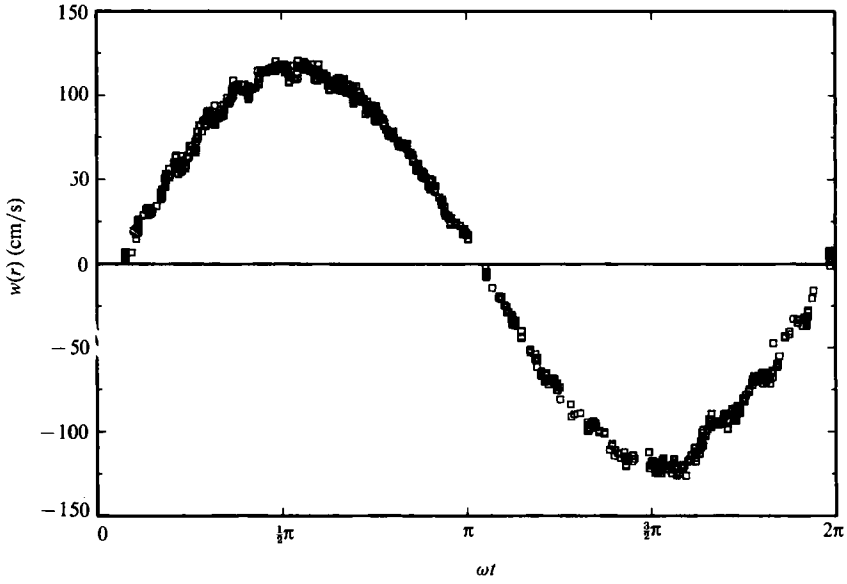

FIGURE 5. Laminar LDV velocity measurement made at dimensionless radial position $r = 0.39$ for $\alpha = 28.0$, $A = 21.6$, $R_\delta = 854$. Dimensionless Stokes-layer thickness is $\delta/a = 0.05$

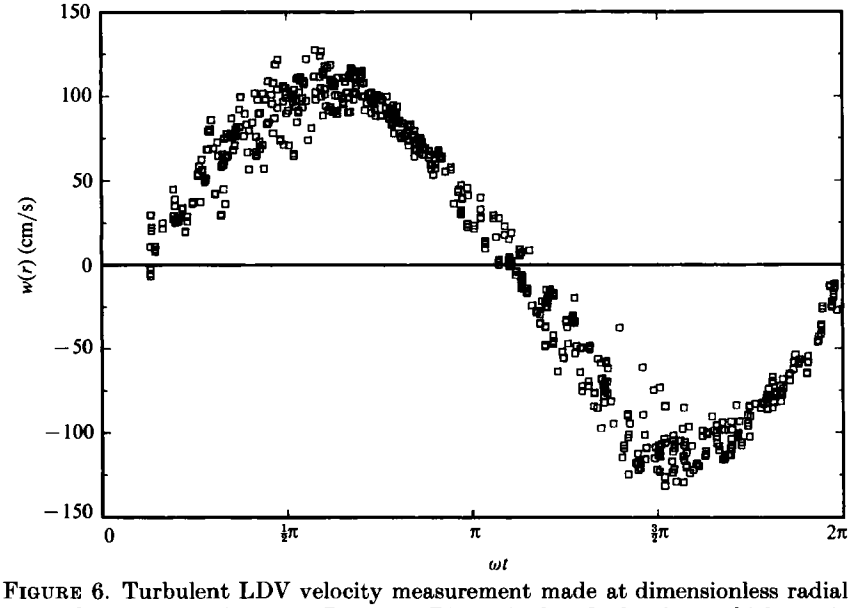

FIGURE 6. Turbulent LDV velocity measurement made at dimensionless radial position $r = 0.88$ for $\alpha = 28.0$, $A = 21.6$, $R_\delta = 854$. Dimensionless Stokes-layer thickness is $\delta/a = 0.05$

position $r = 0.39$. The parameters for this experiment are $\alpha = 28.0$, $A = 21.6$ and $R_\delta = 854$. The distortion of the sinusoid during the first quarter-cycle is caused by a slight rocking in the piston assembly during the upstroke, but the last half-cycle shows the downstroke to be smooth. A sharp spatial transition exists between velocities which graphically appear laminar and those which have the deceleration phase behaviour characterized by Hino *et al.* (1976). An example of this is given in figure 6, in which raw data are displayed for measurements made at $r = 0.88$ for the same parameter values as those used in figure 5. Increased scattering in the data

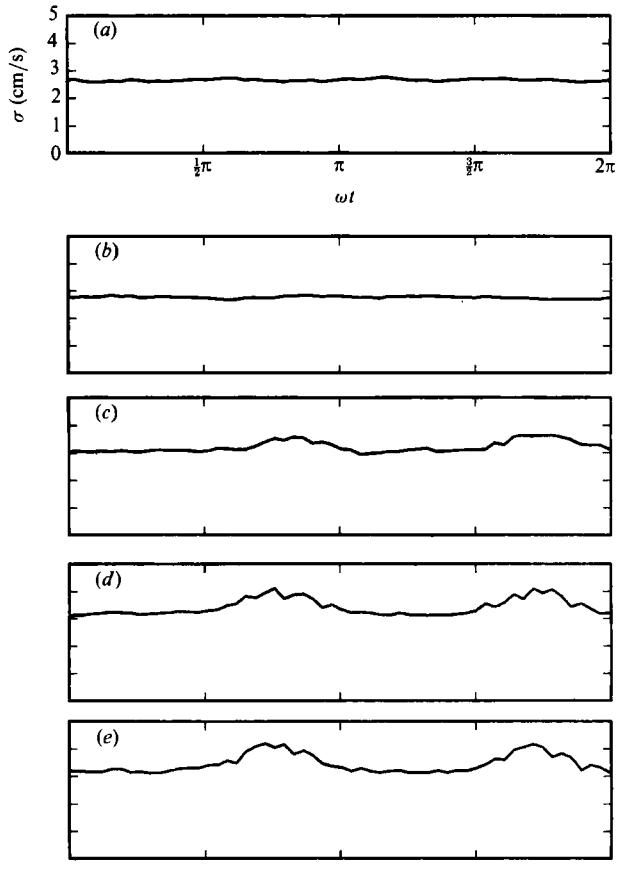

FIGURE 7. $\sigma(r, \omega t)$ for $\alpha = 28.0$, $A = 21.6$, $R_\delta = 854$, $\delta/a = 0.050$. (*a*) $r = 0$. (*b*) $r = 0.39$. (*c*) $r = 0.76$. (*d*) $r = 0.85$. (*e*) $r = 0.88$.

suggests that there is an instability which arises during the decelerative phase of fluid motion, but this instability does not persist during the acceleration phase. The data scattering diminishes and the flow appears to relaminarize during the accelerative part of the oscillatory cycle, as previously observed. We have found, however, that the instability does not penetrate throughout the cross-section, as shown in figure 7 (*a–e*). This figure depicts $\sigma(r, \omega t)$ at various radial positions for the same parameter values used in figures 5 and 6. We see in figure 7 (*c–e*) an increase and subsequent decrease in σ corresponding to generation of turbulence during the decelerative phases for $\frac{1}{2}\pi < \omega t < \pi$ and again for $\frac{3}{2}\pi < \omega t < 2\pi$. The amplitude is greatest near the tube wall and diminishes toward the centreline. The disturbance appears earliest near the wall and propagates inward. Data from other radial positions show the edge of the turbulent annulus to be at $r = 0.68$. Figure 7 (*a–b*) indicates that the turbulence generated in the decelerative phase does not penetrate into the core region of the flow, since σ remains a constant phase independent 3% of U_{rms} at these two radial positions.

This finding is generalized for all $R_\delta > 500$ investigated in this study. As shown in figure 8 (*a–e*) for $\alpha = 20.3$, $A = 19.2$ and $R_\delta = 550$, σ has the same graphical appearance as in figure 7 (*a–e*). The amplitude of σ varies only slightly during deceleration at the dimensionless radial position $r = 0.82$ in figure 8 (*c*), whereas the

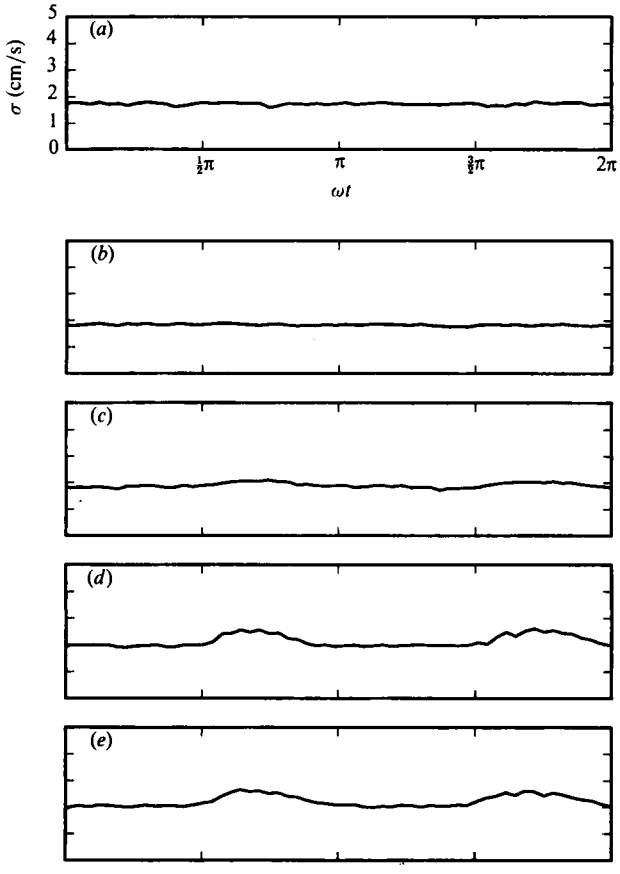

FIGURE 8. $\sigma(r, \omega t)$ for $\alpha = 20.3$, $A = 19.2$, $R_\delta = 550$, $\delta/a = 0.069$. (*a*) $r = 0$. (*b*) $r = 0.76$. (*c*) $r = 0.82$. (*d*) $r = 0.88$. (*e*) $r = 0.92$.

variation is still quite appreciable at $r = 0.76$ in figure 7(*c*). At the centreline σ is independent of the piston phase and is approximately constant at 1.74 cm/s while $\sigma/U_{\text{rms}} = 4.1\,\%$.

From the measured velocities we construct the stability diagram given in figure 9. We have found two regions in the (α, R_δ)-stability plane: a laminar regime, in which the volume-cycled oscillatory flow is stable; and a turbulent boundary-layer regime, in which turbulence occurs during the decelerative phase of fluid motion. Transition from laminar flow to the turbulent boundary-layer flow occurs at $R_\delta = 500$, which is in accord with the value determined by Sergeev (1966) and slightly lower than the value found by Li (1954). Our results differ from those of Hino *et al.* (1976), whose data are also included in figure 9 and described qualitatively above, in that we have not identified a weakly turbulent regime, as did they, and that we have found the turbulence to be present only in an annular region several Stokes layers thick near the wall for these larger values of α. These findings are consistent with Hayashi & Ohashi (1982), Hino *et al.* (1983) and Sumer *et al.* (1987), all of whom demonstrate that, for $\alpha \gg 1$, the Stokes layer becomes turbulent and that the generated turbulence is convected radially inward at R_δ far above transition.

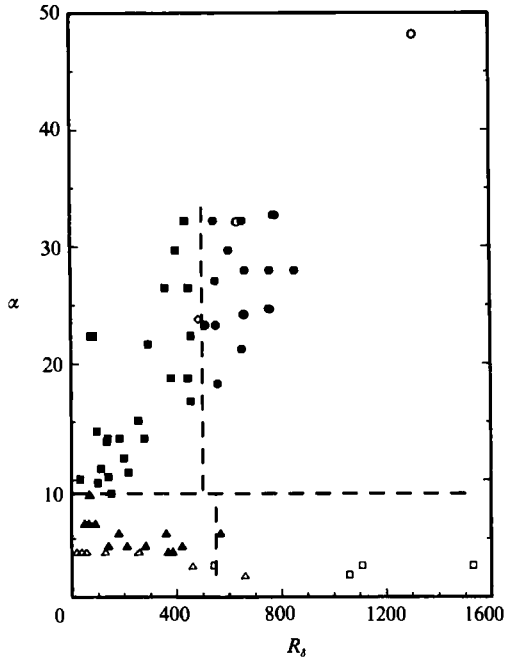

FIGURE 9. $\alpha - R_\delta$ Stability plane determined by LDV measurements. Regimes are: ■, LDV laminar; ●, LDV turbulent boundary layer; ◇, hot-film laminar; ○, hot-film turbulent boundary layer. Hino *et al.* (1976): △, laminar; ▲, weakly turbulent; □, turbulent.

4. LDV measurements near a flow probe

4.1. *Modified experimental apparatus*

The experimental apparatus used in these experiments is the same as that used in the previous experiments with one modification: a hot-wire probe dummy is introduced into the flow through the back side of the Plexiglas test section. A two-axes miniature manual positioning table was mounted to the unistrut support frame such that the two traverse directions were parallel to the face of the Plexiglas test section. When these components were properly aligned, a TSI model 1158 hot-wire anemometer probe was pushed through the Plexiglas plate into the tube. Its penetration depth into the tube was held fixed by a set screw. The features of the hot-wire probe used in these experiments are: the shaft is 0.125 in. in diameter; the needles are 0.375 in. long and are separated by 1.5 mm at the tip; the wire diameter is 0.003 in. The probe shaft is long enough to allow the wire to be positioned anywhere along the front-to-back diameter of the tube. The wire thickness is identical to the hot-film thickness in the third set of experiments discussed in §5. No velocity measurements are taken with this dummy probe in the present experiments. It is resident in the flow only for the purpose of assessing its influence on the nature of the flow as measured by laser-Doppler velocimetry.

Procedural steps almost identical to those followed in the first set of experiments were used in this second set of experiments. We utilize the same measuring and data acquisition systems. The major difference between the two sets of experiments involves the method of positioning of the LDV measuring volume, since these experiments are aimed at determining the influence of the hot-wire probe on the flow. The LDV system was operated with the measuring volume at the tube centre. The

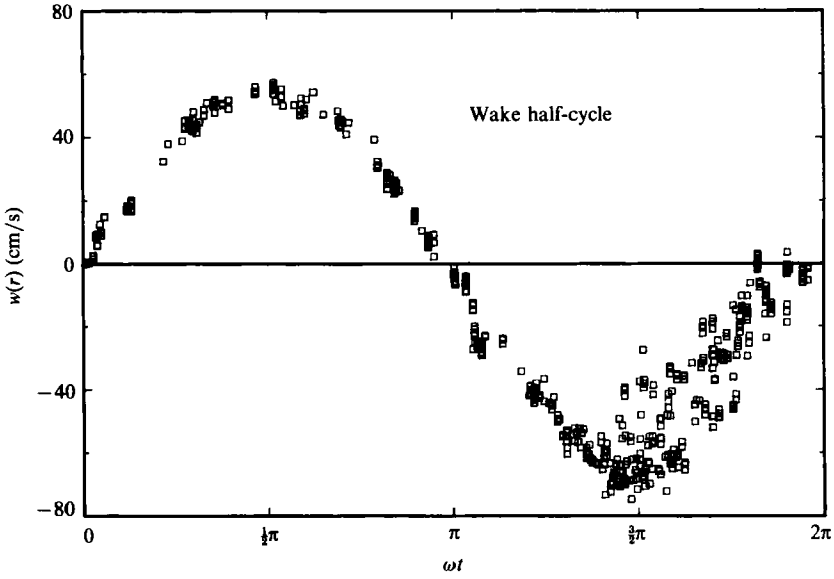

FIGURE 10. LDV velocity measurement with dummy hot-wire anemometer probe. Instability occurs during the wake half-cycle. $\alpha = 23.3$, $A = 16.8$, $R_\delta = 554$, $Z = -0.5$ mm.

hot-wire probe was advanced into the tube until the wire, oriented perpendicular to the flow direction, occupied the measuring volume. This was determined by observation of the imposed frequency-shift frequency on the oscilloscope, the characteristic marker of a stationary object present in the measuring volume. The measuring volume was then traversed sequentially to positions $Z = \pm 0.20$ mm, $Z = \pm 0.50$ mm, $Z = \pm 1.5$ mm and $Z = \pm 5.00$ mm. Measurements of velocity were made at these positions along the axis of the tube for several combinations of A and α used in the first set of experiments. For certain combinations of A and α, velocity measurements were made with the measuring volume/hot-wire configuration at the tube centre and in the boundary layer, or at the boundary layer alone.

4.2. *Data analysis and results*

The data from these experiments were visually displayed on the PDP 11/23+ terminal screen. No regressions of the data were performed, as we could readily assess the presence of a disturbance similar to the turbulence detailed in §3.2 above by visual inspection alone. Measurements made at axial positions of ± 1.5 mm and further from the hot-wire probe did not show any influence of the probe for the α–A parameter combinations examined. The measurements made at the tube centre near the wire ($|Z| < 1$ mm) have one of two characteristics: either the flow is undisturbed, which occurs for $R_\delta < 500$; or the flow has the same type of velocity fluctuations as seen in the turbulent boundary layer described in §3.2. While this behaviour occurs for $R_\delta > 500$, it differs from the turbulent boundary-layer results in that the instability occurs only during the wake half of the oscillatory cycle. The fluid moves past the LDV measuring volume and then past the wire during one half of the cycle, but during the flow reversal phase, fluid first passes the wire and then passes through the measuring volume. It is during the decelerative portion of this half of the oscillatory cycle that the instability appears, as shown in figure 10. Here the instability occurs during the last quarter of the oscillatory cycle since the measuring

R_δ	α	A	Instability? Core/B.L.
554	23.3	16.8	Yes/---
551	27.1	14.4	Yes/---
553	20.3	19.2	Yes/---
559	18.3	21.6	Yes/---
445	18.8	16.8	No/Yes
456	22.4	14.4	No/Yes
382	18.8	14.4	---/Yes
360	26.5	9.6	---/Yes
294	21.7	9.6	---/No

TABLE 2. Occurrence of core and boundary-layer instability in the wake of the dummy hot-wire probe

volume is positioned at an axial position $Z = -0.5$ mm, which is beneath the wire. The instability occurs during the second quarter-cycle when the measuring volume is traversed to a location above the hot-wire probe. Thus, it must be that the wire is tripping an instability in this experiment. However, it does not appear that the vorticity instability is convected back over the wire during the reverse-flow portion of the cycle, although the thermal disturbance may do so.

The parameter values used in these experiments are summarized in table 2. For those values of R_δ for which there was no instability detected in the core flow, the hot-wire probe was placed into the boundary layer at the entry port and LDV measurements were made as described above. Phenomena similar to those occurring in the core region were recorded. Far from the wire the flow was undisturbed, but near the wire the flow was characterized by a wake half-cycle instability, as before. The results are shown in table 2, where the dashes indicate that measurements were not made, either because the boundary layer was known to be turbulent without the hot-wire probe for the parameters indicated or because the core flow did not become unstable with the wire present for higher values of R_δ. Additional measurements were made at lower values of R_δ and it was found that the boundary-layer instability disappeared at $R_\delta = 294$ with the probe resident. These results suggest that the hot-wire probe trips turbulence, as measured by the LDV, in the boundary layer at a lower value of the Reynolds number than that value at which it would otherwise occur.

5. Hot-film anemometer experiment

5.1. *Experimental apparatus*

In this experiment the LDV system is not used and the dummy probe described in §4.1 was replaced by a TSI model 1210–20W hot-film anemometer probe connected to a TSI model 1054A constant temperature anemometer module and a TSI model 1051 power supply and monitor, shown in figure 1. The physical dimensions of the hot-film probe are the same as those of the dummy probe except that a shorter probe shaft restricts positioning of the film to a region no further than one inch from the entry port. Because the hot film is easily damaged by the aqueous salt solution, degassed water is used as the working fluid. Hot-film measurements are made with the two film positions being at the tube centre and near the entry port at a dimensionless radius of 0.95. The combinations of parameters are: $A = 14.4$, $\alpha = 23.8$ ($R_\delta = 485$);

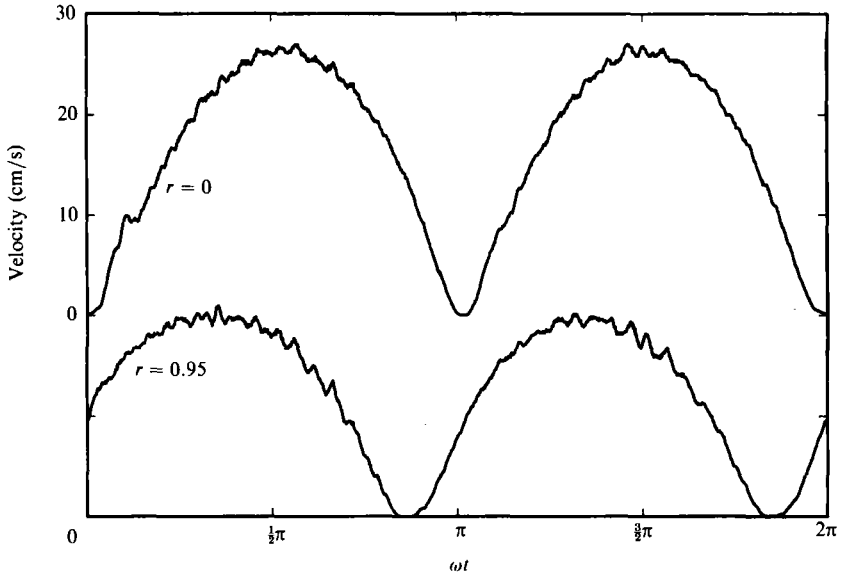

FIGURE 11. Hot-film anemometer velocity at dimensionless radial positions $r = 0$ and $r = 0.95$ for $A = 14.4$, $\alpha = 23.8$, $R_\delta = 485$.

$A = 14.4$, $\alpha = 31.2$ ($R_\delta = 635$); and $A = 19.2$, $\alpha = 48.2$ ($R_\delta = 1310$). Analog output from the anemometer module is both displayed on the oscilloscope and digitally sampled at a rate of 500 Hz by the Data Translation DT2781 A/D converter in the computer. The signal from the synchronization pulse generator is also digitally sampled simultaneously.

5.2. *Results*

The Reynolds numbers and probe positions employed in these measurements were selected to examine the hot-film signal in the core and in the boundary layer at subcritical and supercritical Reynolds numbers, as determined by LDV, and the results of these measurements are included in figure 9. Figures 11–13 show one period of the digitally sampled probe output versus piston phase angle for the two radial probe positions used for each α–A pair. Figure 11 shows the hot-film output to be the expected rectified sinusoid. The two curves are phase-locked to the piston motion, with the upstroke beginning at $\omega t = 0$. The features of the two curves are very similar in appearance for this subcritical case of $R_\delta = 485$. The recording from the boundary layer is smaller peak to peak than the core recording, and is phase-shifted relative to it. There is no indication that this flow becomes unstable in the deceleration phase, although there is a small-amplitude, high-frequency velocity variation in the upstroke and downstroke half of each cycle, perhaps corresponding to weak turbulence or vibrations in the drive apparatus or probe assembly. Thermal anemometer signals typically have the steepest voltage increase and the greatest sensitivity at zero velocity. That the cusp regions in figure 11 are relatively smooth is indicative of the lack of mechanical disturbance caused by the motor assembly during this portion of the cycle.

Figure 12, however, shows a marked difference between the core and boundary-layer recordings for $R_\delta = 635$. The velocity recorded at $r = 0.95$ shows a periodic variation which is more pronounced during the upstroke half of the cycle. During both the upstroke and downstroke we see that the flow accelerates and then the

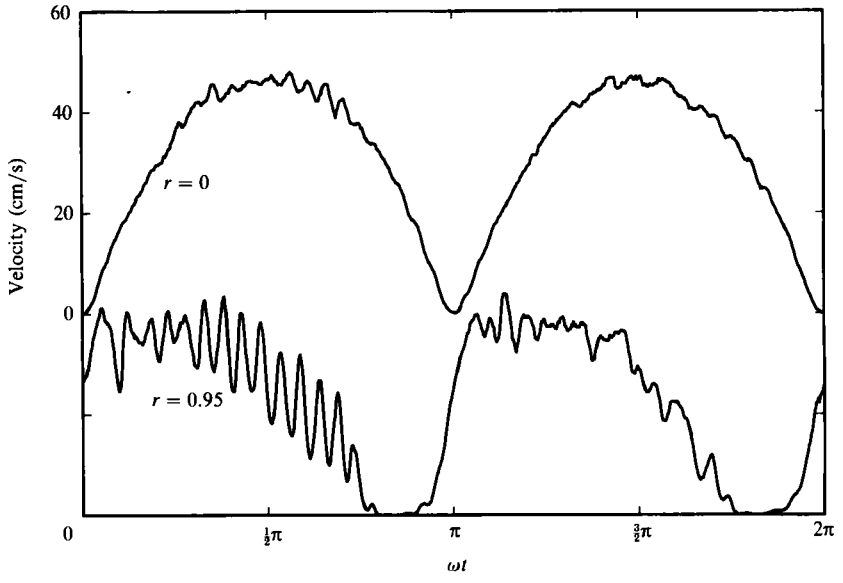

FIGURE 12. Hot-film anemometer velocity at dimensionless radial positions $r = 0$ and $r = 0.95$ for $A = 14.4$, $\alpha = 31.2$, $R_\delta = 635$.

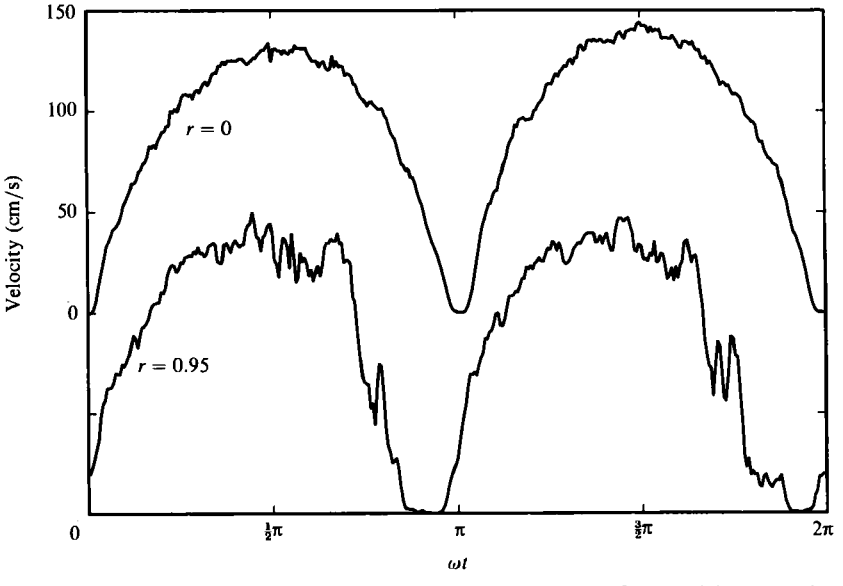

FIGURE 13. Hot-film anemometer velocity at dimensionless radial positions $r = 0$ and $r = 0.95$ for $A = 19.2$, $\alpha = 48.2$, $R_\delta = 1310$.

signal is rather abruptly truncated. This blunting of the probe output signal is strongly associated with measurements in turbulent flows, and is observed in Hino *et al.* (1976). There are relatively large variations in the signal during the deceleration phase of fluid motion, also indicating the onset of an instability. Finally, the cusps lack the smooth appearance previously noted, indicating that a flow disturbance exists in the boundary layer. The recording at $r = 0$ still has smooth cusps, but the

upstroke signal has a wobble which is not as evident during the downstroke half of the cycle. An audible vibration occurring in the drive mechanism coincides with this wobble, which appears near the peak piston velocity. It is important to note that there is no audible wobble when the hot-wire probe resides only within the boundary layer (near the entry port), suggesting that the presence of the probe across the flow causes a large disturbance.

The data in figure 13, $R_\delta = 1310$, show the continued turbulent characteristics in the boundary layer that were described in figure 12, while the data from $r = 0$ is even smoother than the corresponding measurement in figure 12. This is consistent with the core remaining inviscid and stable while the boundary layer is unstable. In this particular experiment, the entrance length for a laminar boundary layer calculated by the criterion of Gerrard & Hughes (1971) is 49 in. Our apparatus measures 52 in. from the junction of the cone and the lower connecting tube to the probe. However, the distance from the free surface to the probe has a minimum of 36 in. and a maximum of 48 in. There appears to be no 'entrance effect' from the free surface under these conditions, probably a result of the shorter entrance length necessary for development of the turbulent boundary layer.

6. Conclusions

In this study we are concerned with defining the conditions under which transition to turbulence will occur. As Taylor (1915) and Prandtl (1921) determined, viscous processes are necessary for the initial instability in non-flexional shear flows. In the absence of viscosity, such as in the core region of high α pipe flow, Rayleigh's analysis (1887) illustrates that an inflexion point in the velocity field is necessary for there to be an instability. For sufficiently large Womersley parameter, laminar theory predicts that viscous effects are confined to the Stokes layer and the central core is an irrotational plug flow. It would be expected, then, that the onset of a flow instability would appear in the region of the velocity field where large velocity gradients exist, and that any study of transition to turbulence in oscillatory flow should thus concern itself primarily with examining the stability of the viscous boundary layer.

To determine if the results of previous hot-wire studies of oscillatory tube flow accurately reflect the actual fluid mechanical events occurring, it is necessary to consider the various mechanisms by which the hot-wire measurements can be skewed. Perhaps the most obvious of these effects is disturbance of the flow caused by the presence of the measuring probe, as noted by Merkli & Thomann (1975). In an oscillatory flow the probe is potentially always 'sitting in its own wake', such that downstream disturbances (either vorticity or thermal) caused during one half of the oscillatory cycle may be convected back over the wire during the other half of the cycle. We measured no turbulence being convected back over the LDV measuring volume, 1 mm upstream of the probe, however the reversing wake need only provide a source of local vorticity to supply the ingredients for an instability. At lower values of α, such as those used in Hino *et al.*'s (1976) experiments, the boundary layer is thick enough for there to be vorticity in the flow far from the wall, even without the probe.

In addition, although it is generally supposed that heat transferred to the fluid dissipates rapidly into the surrounding fluid, recent studies of Elger & Adams (1987) in dynamic hot-wire calibration in oscillatory flows suggest that this may be an important effect after all. Paired with the comments of Merkli & Thomann (1975)

who demonstrate that the hot-wire probe visibly disturbs the flow, there is strong reason to believe that the nature of the flow at transition to turbulence has not been well established. Certainly, an understanding of the onset as well as the spatial and temporal distribution of turbulence is important to the correct development of the transport phenomena fundamental to physiological, as well as other flows.

From our preliminary experiments we have shown that the experimental apparatus has been constructed to provide an axisymmetric oscillatory flow free from most mechanical vibration and end effects. The working fluid for LDV measurements has been selected according to appropriate criteria and has been demonstrated to be both Newtonian and independent of intrusive effects of the laser measurement system. The LDV experiments conducted on volume-cycled oscillatory pipe flow show that such a flow is laminar in the parameter range $8.9 \leqslant \alpha \leqslant 32.2$ and $R_\delta < 500$. This value of the Reynolds number is in good agreement with power measurements made by Sergeev (1966) and slightly lower than the observations of Li (1954). For $500 < R_\delta < 1310$, the core flow remains laminar while the Stokes layer becomes unstable during the deceleration phase of fluid motion. This turbulence is most intense near the solid boundary and is detected in an annular region of variable thickness. These results are consistent with those of Hino *et al.* (1983), Hayashi & Ohashi (1982) and Sumer *et al.* (1987) whose investigations demonstrated the same temporal features as our LDV measurements. Our results differ from theirs since we find the instability near transition to be confined to an annular region near the wall while they report that the turbulence generated near the wall gets dispersed across the entire cross-section when R_δ is much greater than the transition value.

Results of LDV measurements made with a dummy hot-wire probe resident in the core flow show that turbulence occurs during the deceleration phase in the wake of the probe for $R_\delta > 500$. Furthermore, this same type of instability is detected in the wake of the wire when the dummy probe is present in the boundary layer for $R_\delta > 300$. This reduction in the critical Reynolds number is consistent with the findings of Merkli & Thomann (1975). Additionally, our hot-film recordings show an instability appearing in the boundary layer while the core flow generally remains smooth for $500 < R_\delta < 1310$.

These results are in accord with theoretical predictions of instabilities occurring in Stokes layers. Neither linear stability theories such as those of Collins (1963), von Kerczek & Davis (1974) and Yang & Yih (1977), nor energy formulations such as those of von Kerczek & Davis (1972) and Davis & von Kerczek (1973) have determined a parameter regime suitable for growth of an instability. It is possible that large-amplitude, three-dimensional disturbances in the flow lead to the boundary-layer instabilities detected, given that nonlinear effects are outside the realm of linear theory. The fact that the spatial and temporal features of the oscillatory flow of a Newtonian viscous fluid have been identified by non-intrusive means in these experiments, and that the spatial features differ significantly from previous results suggests that models of heat or mass exchange relying on this flow field should be re-examined. Such models must incorporate the fact that, while the flow becomes unstable only during part of the oscillatory cycle, it is only a boundary layer which exhibits the instability. The turbulent mixing is confined to a well-bounded annulus of variable thickness during the decelerative phase for $500 < R_\delta < 1310$, as determined in this study. The functional dependence of this turbulent mixing layer on the flow parameters remains undetermined, but for sufficiently large R_δ it has been shown by other investigators to encompass the entire cross-section. This turbulent mixing layer is coupled to an inviscid core flow, and the

net axial transport of a soluble contaminant will rely on the interaction of the inviscid core with the viscous/turbulent boundary layer.

This research was funded by NIH grants K04-HL01818, R01-HL41126, 2R01-HL35440 and NSF grants MSM-8351494 in conjunction with General Motors Corporation. The experiments were conducted in the Northwestern University Center for Multiphase flow and Transport. We wish to acknowledge the valuable advice of Dr Alan Kistler, Dr Donald P. Gaver III, Mr Douglas Kerns and Mr Michael Lund.

REFERENCES

COLLINS, J. I. 1963 Inception of turbulence at the bed under periodic gravity waves. *J. Geophys. Res.* **18**, 6007–6014.

COOPER, E. R., JANKOWSKI, D. F., NEITZEL, G. P. & SQUIRE, T. H. 1985 Experiments on the onset of instability in unsteady circular Couette flow. *J. Fluid Mech.* **161**, 97–113.

DAVIS, S. H. & VON KERCZEK, C. 1973 A reformulation of energy stability theory. *Arch. Rat. Mech. Anal.* **52**, 112–117.

ECKMANN, D. M. & GROTBERG, J. B. 1988 Oscillatory flow and mass transport in a curved tube. *J. Fluid Mech.* **188**, 509–527.

ELGER, D. F. & ADAMS, R. L. 1987 Dynamic hot wire calibration in an oscillating flow. *Bull. Am. Phys. Soc.* **32**, 2106.

FREDBERG, J. J. 1980 Augmented diffusion in the airways can support pulmonary gas exchange. *J. Appl. Physiol.: Respirat. Environ. Exercise Physiol.* **49**, 232–238.

GERRARD, J. H. & HUGHES, M. D. 1971 The flow due to an oscillating piston in a cylindrical tube: a comparison between experiment and a simple entrance flow theory. *J. Fluid Mech.* **50**, 97–106.

GODLESKI, D. A. & GROTBERG, J. B. 1988 Convection-diffusion interaction for oscillatory flow in a tapered tube. *Trans. ASME* K: *J. Biomech. Engng* **110**, 283–291.

HAYASHI, T. & OHASHI, M. 1982 A dynamical and visual study on the oscillatory turbulent boundary layer. In *Turbulent Shear Flows 3* (ed. L. J. S. Bradbury, F. Durst, B. Launder *et al.*), pp. 18–33. Springer.

HINO, M., KASHIWAYANAGI, M., NAKAYAMA, A. & HARA, T. 1983 Experiments on the turbulence statistics and the structure of a reciprocating oscillatory flow. *J. Fluid Mech.* **131**, 363–400.

HINO, M., SAWAMOTO, M. & TAKASU, S. 1976 Experiments on transition to turbulence in an oscillatory pipe flow. *J. Fluid Mech.* **75**, 193–207.

JOSHI, C. H., KAMM, R. D., DRAZEN, J. M. & SLUTSKY, A. S. 1983 An experimental study of gas exchange in laminar oscillatory flow. *J. Fluid Mech.* **133**, 245–254.

KERCZEK, C. VON & DAVIS, S. H. 1972 The stability of oscillatory Stokes layers. *Stud. Appl. Math.* **51**, 239–252.

KERCZEK, C. VON & DAVIS, S. H. 1974 Linear stability theory of oscillatory Stokes layers. *J. Fluid Mech.* **62**, 753–773.

KURZWEG, U. H. 1985 Enhance heat condition in fluids subjected to sinusoidal oscillations. *J. Heat Transfer* **107**, 459–462.

LI, H. 1954 Stability of oscillatory laminar flow along a wall. *Beach Erosion Bd., US Army Corps of Engineers Tech. Memo.* 47.

MERKLI, P. & THOMANN, H. 1975 Transition to turbulence in oscillating pipe flow. *J. Fluid Mech.* **68**, 567–575.

OHMI, M., IGUCHI, M., KAKEHASHI, K. & MASUDA, T. 1982 Transition to turbulence and velocity distribution in an oscillating pipe flow. *Bull. JSME.* **25**, 365–371.

PRANDTL, L. 1921 Bemerkungen euber die Entstehung der Turbulenz. *Z. angew. Math. Mech.* **1**, 431–436.

RAYLEIGH, LORD 1887 On the stability, or instability, of certain fluid motions. 2. *Scientific Papers*, vol. 3, pp. 2–23. Cambridge University Press.

SERGEEV, S. I. 1966 Fluid oscillations in pipes at moderate Reynolds numbers. *Trans. Sov. Fluid Dyn.* **1**, 121–122.

SLUTSKY, A. S., DRAZEN, J. M., INGRAM, R. H., KAMM, R. D., SHAPIRO, A. H., FREDBERG, J. J., LORING, S. H. & LEHR, J. 1980 Effective pulmonary ventilation with small-volume oscillations at high frequency. *Science* **209**, 709–611.

SMITH, R. 1982 Contaminant dispersion in oscillatory flows. *J. Fluid Mech.* **114**, 379–398.

SUMER, B. M., JENSEN, B. L. & FREDSOE, J. 1987 Turbulence in oscillatory boundary layers. *Advances in Turbulence.*

TAYLOR, G. I. 1915 Eddy motion in the atmosphere. *Phil. Trans. R. Soc. Lond.* A **215**, 1–26.

WATSON, E. J. 1983 Diffusion in oscillatory pipe flow. *J. Fluid Mech.* **133**, 233–244.

YANG, W. H. & YIH, C.-S. 1977 Stability of time-periodic flows in a circular pipe. *J. Fluid Mech.* **82**, 497–505.